Dielectric properties of single crystal spinels in the series FeV_{2}O_{4}, MnV_{2}O_{4}, and CoV_{2}O_{4} in high magnetic fields

A. Kismarahardja, J. S. Brooks, H. D Zhou, E. S. Choi, K. Matsubayashi, and Y. Uwatoko

Phys. Rev. B **87**, 054432 — Published 27 February 2013

DOI: 10.1103/PhysRevB.87.054432

Dielectric Properties of Single Crystal Spinels in the series FeV_2O_4, MnV_2O_4 and CoV_2O_4 in High Magnetic Fields

A. Kismarahardja[1,2*], J.S. Brooks[1], H.D Zhou[1], E.S. Choi[1], K. Matsubayashi[3], and Y. Uwatoko[3]

[1]Dept. of Physics and National High Magnetic Field Laboratory,
Tallahassee, Florida, 32310 USA

[2]STKIP Surya (Surya Research and Education Center),
Gading Serpong, Tangerang 15810, Indonesia

[3]The Institute for Solid State Physics, The University of Tokyo, Kashiwa, Chiba 277-8581, Japan

Monday, February 04, 2013

Abstract

We report a comparative investigation of the magnetostrictive and magnetoconductivity effects in the low temperature ferrimagnetic phases of the spinel vanadate structure AV_2O_4 where A = Fe, Mn, and Co. In FeV_2O_4 both the Fe and V sites have orbital degrees of freedom, the V-V distance places the compound intermediate between localized and itinerant charge carrier behavior, and there are three structural and two magnetic transitions vs. temperature. For MnV_2O_4 and CoV_2O_4, only the V-sites have orbital degrees of freedom. MnV_2O_4 has the largest V-V distance and the most localized conductivity, with one structural and one magnetic transition. CoV_2O_4 has the shortest V-V distance, and approaches the itinerant charge carrier threshold. CoV_2O_4 has one ferrimagnetic transition and no long range ordered structural transition. Working with single crystals, ac dielectric and resistance measurements vs. temperature and magnetic field exhibit distinctive physical properties in each case. These include the magneto-caloric signatures of magnetization reversal (Fe and Co), separable isotropic and anisotropic magnetostrictive effects (Mn), glass-like dynamics (Co), and evidence in the field-dependent dielectric response for the alteration of the ferrimagnetic spin structure with increasing

magnetic field (Fe). These findings can guide future dielectric- and magnetoconductance- based spinel studies with a focus on the low temperature and high magnetic field properties of canted ferrimagnetic spin configurations and orbital-lattice ordering effects.

PACS numbers 75.25.+z, 76.60.-k, 75.10.-b, 75.50.Gg, 75.80.+q, 71.70.Ej

* Corresponding Author.

adewijaya80@yahoo.com

I. INTRODUCTION

Transition metal oxide compounds of the spinel AB_2O_4 type have long been a subject of considerable activity[1], enhanced by the emerging interest in spin frustration and critical point phenomena[2], and most recently by deeper insight into ferrimagnetic[3, 4] and ferroelectric[5] structure, orbital ordering[6], magnetocaloric[7] and glassy effects[8]. The essential features of the spinel structure include the oxygen sharing tetrahedrally-coordinated A-sites, and the octahedrally-coordinated B-sites (Fig. 1a). The coordination removes the 5-fold degeneracy of the 3d levels, producing the triply degenerate t_{2g} and doubly degenerate e_g levels. The energy of these levels depends on the coordination: for the A (B) sites, $t_{2g} > e_g$ ($e_g > t_{2g}$). With different d-electron fillings, the spin of the A and B sites will change, and where a set of degenerate levels are not completely filled, orbital degrees of freedom are possible. Since orbital symmetry is coupled to the lattice, spin-orbital coupling can produce correlations between magnetic order and the lattice strain. In addition, temperature and magnetic field can induce distortions of the tetrahedral and octahedral symmetries that can further remove degeneracy in the e_g and t_{2g} levels, thereby inducing further changes in the orbital and lattice configurations[9].

There is a hierarchy of magnetic and structural (and orbital) properties in the AV_2O_4 series. *(i)* Starting with a non-magnetic ion in the A-site (such as Cd, Zn, Mg) the magnetic ground state involves antiferromagnetic order on the pyrochlore V-sites (Fig. 1b), which due to spin frustration[4], occurs at a temperature T_N less than the Curie-Weiss constant θ_W, where $|\theta_W|/T_N > 1$ is a measure of the frustration (e.g. ~ 400 K/90 K for A = Cd[10]). More precisely, a Jahn-Teller (J-T) distortion in the cubic lattice breaks the symmetry of the octahedral sites, causing orbital order (a cubic to tetragonal structural transition), and this in turn produces one-dimensional spin chains that can then develop antiferromagnetic long range order and a magnetic

transition at a lower temperature T_C [10]. (ii) When the A-site has a magnetic ion (A = Mn, Co), there can be A-V magnetic interactions, and this can alter the V-site moments, producing ferrimagnetic order in the A-V system. (Estimates of the magnetic interactions[11] for MnV_2O_4 are: $J_{V\text{-}V}$ = +20 K, $J_{Mn\text{-}V}$ = - 9 K, and $J_{Mn\text{-}Mn}$ = -0.3 K.) These interactions can also influence the orbital and lattice configurations at the V-site. *(iii)* The ferrimagnetic transition temperature T_C and electrical transport activation energy E_a are shown for A = Mn, Fe, and Co in Fig. 1c (see also Fig. 2a for temperature dependent resistivity). As the V-V distance decreases with either chemical or physical pressure, the magnetic transition temperature increases and the activation energy of charge carriers decreases. Further, our work[12] and that of others[8] suggests that orbital (and structural) order may also go from long-range to short-range with a decrease in V-V distance, thereby suppressing the structural transition. *(iv)* When the A-ion is magnetic and in addition has orbital degrees of freedom (as with A = Fe), the orbital, structural, and magnetic properties become more complicated, and magnetostrictive effects are of opposite sign (compared with A = Mn, Co), with respect to magnetic field direction.

Mobile carriers also play a role in the AV_2O_4 physics and in ac dielectric measurements. For instance in the case of MnV_2O_4, band structure [13] and thermopower measurements[11] indicate that the electrical conductivity is primarily due to mobile holes that are activated from V t_{2g} bands lying in the immediate proximity of the Fermi level. A gap of 1.1 eV separates the Fermi level from the next highest energy bands. However the activation energies derived from electrical transport in these materials[12, 14] are characteristically much smaller (of order 300 meV or less), and mechanisms such as the effects of the Weiss field[15] on bands near the Fermi level may account for an energy scale significantly less than the band gap. The activated

conductivity is influenced by magnetic and orbital changes, and temperature and field dependent dielectric and conductance measurements are therefore sensitive to phase transitions.

Our work to date has included the pressure-induced metallic behavior in CoV_2O_4 which sits at the boundary of itinerant electron behavior[14], and a study of the chemical pressure dependence of the structural and magnetic transitions in $Mn_{1-x}Co_xV_2O_4$ [12]. In the work reported here we focus on three spinel vanadates whose properties depend on orbital ordering and inter-vanadium distance R_{V-V}. In all three AV_2O_4 compounds studied, the V^{3+} site is octahedrally coordinated with oxygen, leading to low lying partially empty t_{2g} levels. This leads to orbital degrees of freedom in addition to the S = 1 moment on the V^{3+} ion. The A ions are tetrahedrally coordinated with oxygen, leading to low lying e_g orbitals. Here Mn^{2+} is spin 5/2, Co^{2+} is spin 3/2, and Fe^{2+} is spin 2. However, only in FeV_2O_4 is orbital order present on the A-site (Fe) as well as on the B-site (V).

The report below is organized as follows. The experimental methods are presented, and since the interpretation of the measurements presented depends on an understanding of the dielectric signal, we first discuss the dielectric response of FeV_2O_4 (R_{V-V} = 2.99 Å, ρ(RT) ~ 55 Ω cm), which shows the most pronounced effects in magnetic field. We then treat each of the remaining two compounds in order of their inter-vanadium distance R_{V-V}, MnV_2O_4 (R_{V-V} = 3.014 Å, ρ(RT) ~ 220 Ωcm) and CoV_2O_4 (R_{V-V} = 2.973 Å, ρ(RT) ~ 0.065 Ωcm). Next we discuss the main findings of our investigation, and summarize by emphasizing the fertile ground for future studies at low temperatures and high magnetic fields.

II. EXPERIMENTAL

Single crystals of AV_2O_4 (A = Mn, Fe, or Co) were grown by the traveling-solvent floating zone technique. The feed and seed rods for the crystal grown were prepared by solid state reaction. Appropriate mixtures of A_2O_3, A, and V_2O_3 were ground together and pressed into 6-mm-diameter 60-mm rods under hydrostatic pressure 400 atm and then calcined in vacuum in a sealed quartz tube at 1000^{o}C for 12 hours. The crystal growth was carried out in argon in an IR-heated image furnace equipped with two halogen lamps and double ellipsoidal mirrors with feed and seed rods rotating in opposite direction at 25 rpm for a crystal growth rate of 30 $^{mm}/_{h}$. Due to the evaporation of V_2O_3 during the growth, extra V_2O_3 in the starting material and high growth speeds are critical to obtain high quality samples. X-ray diffraction (XRD) refinement shows that site disorder is less than 5 % in the samples studied in this work. For FeV_2O_4, refinement of neutron diffraction data on polycrystalline samples[3] has indicated a site inversion of Fe onto the V site of $Fe[Fe_{0.058}V_{0.942}]_2O_4$. Although no compositional analysis was performed, it is expected that in general the stoichiometry of the single crystal samples used in the present work are similar to that reported by Zhang et al. [5].

The crystals were cut in a rectangular shape with average dimensions 3 x 2 x 1 mm^3 along the $\mathbf{a_1}$, $\mathbf{a_2}$, and $\mathbf{a_3}$ ([100], [010], and [001]) directions of the room temperature cubic lattice. Silver paint electrodes were placed on opposing parallel surfaces, and the magnetic field was applied either perpendicular to the electrode planes along the electric field (B//E), or parallel to the electrode planes perpendicular to the electric field (B⊥E). The crystallographic axes and electric and magnetic field directions for the dielectric studies are shown in Fig. 3. In all cases presented here, the samples were clamped to the G10 probe platform with a 1/16'' thick G10 plate held down at its four corners with set screws. An additional layer of perforated paper and GE varnish was used to buffer the G10-sample electrode interfaces. Hence there was a modest strain on the

sample, which was always in the same direction as the electric field of the electrodes. An Andeen Hagerling (AH) Capacitance Bridge AH 2700 was used to collect the capacitance (C in pF) and dissipation (D in nS) data using a frequency $\omega/2\pi$ = 10 kHz, and a Cernox thermometer located near the crystal was used to measure the temperature. In this report, the dielectric response is presented in several forms, either in terms of C and D, or ε' (= $Cd/\varepsilon_0 A$) and ε'' (= ε' tanδ where tanδ = $D/\omega C$), or in terms of their fractional change, or percentage change. Electrical transport measurements were carried out in both superconducting and high field resistive magnets with standard 4-terminal resistance measurements.

III. RESULTS: DIELECTRIC PROPERTIES OF AV_2O_4 (A = Fe, Mn, Co) IN MAGNETIC FIELDS

A. FeV_2O_4

We first discuss FeV_2O_4 since it exemplifies many of the features of the spinel systems as manifested in dielectric measurements. This spinel has the most complex structural and magnetic behavior of all compounds reported herein due to the existence of orbital degrees of freedom on both the Fe and V sites. There is a cubic-to-tetragonal (HT) transition at T_{HT} = 140 K, a structural HT-to-orthorhombic transition at T_{TO} = 110 K, accompanied by a paramagnetic-to-ferrimagnetic transition T_C at the same temperature, and an orthorhombic-to-tetragonal (LT) transition at T_{LT} = 70 K. At T_C, the ferrimagnetic alignment between the Fe and V spins is collinear along the [001] direction, but recent studies of the magnetic structure by NMR [16] and neutron-diffraction[3] show that below the second structural transition T_{LT}, the V^{3+} magnetic moments become canted approximately along the [111] direction. The temperature dependent resistivity of FeV_2O_4 is shown in Fig. 2a, where due to the rapid increase in resistivity, no structural or magnetic effects

are observable. However, as shown in Fig. 2b the temperature dependence of the dielectric signals for FeV_2O_4 exhibit features associated with the various structural transitions as indicated. Systematic magnetic field dependent dielectric measurements (hysteresis cycles) at constant temperatures spanning the range of these transitions reveal additional features associated with the magnetic, lattice, and itinerant electron properties in these different phases[17]. In this report we focus only on the behavior of FeV_2O_4 in the low temperature tetragonal phase.

In Fig. 3 we show a typical dielectric measurement of a FeV_2O_4 single crystal at a low temperature (4.2 K) well below the structural and ferrimagnetic transitions. With increasing magnetic field, the capacitance is observed to decrease for B//E and to increase for B⊥E. Based purely on geometrical (Poisson) effects where we assume a constant volume condition for a cubic sample in a parallel capacitor geometry[17] this response corresponds to an expansion of the sample dimension along the magnetic field direction ($\Delta C_{//}/C_{//} = -2\Delta L_{//}/L_{//}$) and a contraction perpendicular to the magnetic field ($\Delta C_{\perp}/C_{\perp} = -2\Delta L_{\perp}/L_{//}$), where $\Delta L_{//} = -2\Delta L_{\perp}$. By comparing the change in capacitance ΔC (Fig. 3) from its lowest value near B= 0 to the saturation value for B ~ 5 T, we find $\Delta L_{//}/L_{//} = +1$ % and $\Delta L_{\perp}/L_{//} = -0.4$%, in reasonable agreement with previously reported measurements [3] in FeV_2O_4.

The origin of the hysteresis in Fig. 3 may be due to microdomains with random magnetic polarization for B = 0, which align with increasing field, and the result is that the tetragonal structure of the microdomains is then manifested in the change in sample dimensions. In the case of FeV_2O_4, there is a dramatic release of heat when the domains switch orientation. This is the hallmark of the coercive field B_c where the magnetization M = 0, giving rise to the sharp magnetocaloric transients in the capacitance signal (see discussion below). Here we note that in

the virgin sweep in Fig. 3b where the sample has been zero field cooled (ZFC) from above T_{HT}, the capacitance is constant for small fields, and then begins to change according to magnetostrictive changes, and in subsequent field cycles, a regular hysteresis loop is stabilized. An important point is that in general, the extrema (peaks or dips) of the hysteresis loops correspond to the M = 0 points, coincident with the coercive field $\pm B_c$. Hence even for subsequent field cycles with no virgin sweep history, or in cases where no magnetocaloric effect is evident, the M = 0 positions in the data can be identified. At higher fields, the purely magnetic contribution to the capacitance saturates. Nishihara et al.[18] were the first to report magnetization jumps and hysteresis in FeV_2O_4. This was followed soon after by a report of similar effects by Takei et al. [19] in the capacitance of polycrystalline samples, who reported the presence of a small feature in the magnetization near zero field that was attributed to a moment with a small coercive field (here B_c'). This feature also is observable in some of our results (see inset of Fig. 3a and magnetization in Fig. 3c), and shows that there are at least two domain systems with different coercive fields ($B_c \sim 1$ T; $B_c' \sim 0.01$ T) present at low temperatures.

It was further noted in Ref. [19] that there is a connection between the capacitance signal and the magnetization hysteresis curve, namely $M^2 \sim \Delta C$. In the present work, in single crystalline FeV_2O_4 at low temperatures (were the dissipative signal is negligible) we find there is an almost direct correspondence between the magnetocapacitance signal and the magnetization. This is shown for the B//E data from Fig. 3b in Figure 3c, where we have transformed ΔC into a magnetization hysteresis loop using the relation $M_C \sim \mathrm{sgn}(B_c)*\mathrm{sqrt}(\Delta C)$. (This is just the inverse of $C \sim M^2$ where $\mathrm{sgn}(B_c)$ accounts for the sign reversal of the magnetization between coercive field points in the hysteresis cycle.)

Results on the capacitive (C) and dissipative (D) dielectric response of FeV_2O_4 for B⊥E are shown in Fig. 4a and 4b for temperatures up to the T_{LT} transition at 70 K. FeV_2O_4 begins to exhibit a significant dissipative contribution to the capacitance signal due to thermally activated charge carriers even at 25 K, which grows at higher temperatures. In a simple analysis, the dissipative signal ($D_{dissipative}$), which can be thought of as a magnetoconductance term, is additive with the reactive capacitive term ($C_{reactive}$) to produce the observed capacitive signal $C_{observed} = C_{reactive} + \alpha * D_{dissipative}$, where α is a signal-mixing fraction less than unity. By inspection, $\alpha \sim 0$ at 4.2 K, and the capacitance signal, which corresponds mainly to the magnetostrictive effects, saturates above 4 to 5 T. However, at higher temperatures the capacitive signal shows further monotonic field dependence beyond the magnetic saturation field that directly corresponds to the dissipative (magnetoconductance) behavior, and hence an increase in α. To derive the magnetic hysteresis behavior of FeV_2O_4 from the temperature dependent dielectric data in Fig. 4 we have first extracted $C_{reactive}$ from the capacitance signal as discussed above. We then use the criterion that $C_{reactive}$ saturates at high fields (~ 5 T) to determine the value of α at each temperature. The results in Figure 4c clearly show that the large coercive field goes to zero at the low temperature tetragonal-to-orthorhombic transition at T_{LT}= 70 K. At higher temperatures there is a complex behavior (not shown) of both $C_{observed}$ and $D_{dissipative}$ that change in accord with crossing the different structural and magnetic phase transitions[17]. The dissipation signal in Fig. 4b indicates that the magnetoconductance is negative, i.e. the magnetoresistance (MR) is positive. However, above 70 K, the magnetoconductance abruptly reverses sign and the MR becomes negative[17].

The temperature transient associated with B_c at low temperatures (Fig. 4a and 4b) arises from "friction heating" where the magnetic domains switch direction when M changes sign. Using the measured heat capacity, the temperature dependence of the capacitance (see Fig. 2b) , and the work done on a sample in a hysteresis loop, we estimate the ideal adiabatic rise in temperature of the sample could be very high (temperature differences of order 100K[17]). Although the main thermal recovery is fast (~ 1 s), it is still evident in the slight difference in the capacitance right before and after a switch. The temperature dependence of the magnetic field position of the magnetocaloric spike (Fig. 5a) yields the temperature dependence of B_c, as shown in Fig. 5b along with values derived from the magnetocapacitance ($4.2 \leq T \leq 70$ K - Fig. 4c) and magnetization ($4 \leq T \leq 12$ K – Ref. [17]). B_c decreases with temperature, vanishing at T_{LT}. Since this is the temperature at which the spin configuration changes from non-collinear to collinear, the domain structure associated with B_c must be a result of the non-collinear structure below T_{LT}.

Finally, we report one additional preliminary finding in FeV_2O_4. Although not yet systematically studied, at low temperatures below T_{LT}, and at very high magnetic fields between 5 and 33 T well above the coercive field in FeV_2O_4, we observed a monotonic change in the magnetization as inferred from ΔC (Fig. 6 - compare with Fig. 3a at low fields, also for $B \perp E$). This is accompanied by a significant hysteresis that is persistent up to the highest field. We will return to this high field behavior in the Discussion section.

B. MnV_2O_4

The spinel vanadate MnV_2O_4 undergoes a paramagnetic-to-ferrimagnetic (collinear) transition $T_C = 56$ K, followed by a cubic-to-tetragonal structural transition at $T_S = 52$ K [20] where the ferrimagnetic order becomes non-collinear[21, 22]. The ferrimagnetism is thought to arise from

antiferromagnetic coupling between the A and B sites through oxygen [23]. A recent infrared ellipsometry study[6] suggests that the V t_{2g} orbitals may prefer the antiferro-type orbital ordering. Magnetic fields can induce magnetic and also structural (cubic-to-tetragonal) order in the vicinity of T_C and T_S [23, 24]. A possible model, based on neutron diffraction, is for the Mn spins to align ferromagnetically along a preferred axis, and for the V spins to be aligned, in the opposite direction, but canted [22]. NMR studies show two in-equivalent ^{51}V sites that suggest a superlattice of two different orbitally ordered structures due to two different configurations of the t_{2g} orbitals in the pyrochlore lattice in the tetragonal state below T_S [21].

The magnetocapacitive response for a single crystal of MnV_2O_4 for two magnetic field orientations at 4.3 K are shown is Fig. 7a. For B//E the capacitance increases with magnetic field, indicating a compression of the sample dimension along the field direction. The dissipation signal (not shown) shows a negative magnetoconductance[17]. For B⊥E the capacitance signal is more complicated and the changes are significantly smaller than for B//E, but generally the capacitance decreases. The very large (small), monotonic (complex) signal seen for B//E (B⊥E) indicates the competition of two magnetostrictive effects, one anisotropic, depending on field direction, and the other isotropic, a difference well beyond the factor-of-two expected based on the Poisson arguments in Sect. A above. Under the assumption that there is an isotropic magnetostriction associated only with magnetic field intensity, we have used the capacitance data in Fig. 7a at 4.3 K to separate by subtraction, the anisotropic and isotropic contributions as shown in Fig. 7b and 7c respectively. Our results indicate that the two effects are of comparable size, and since both are hysteretic, their difference (for B⊥E) leads to the smaller, double-peaked signal shape. We note that MnV_2O_4 at 4.3 K shows a change in $\Delta L/L$ of order 0.4% for each of the separate magnetostrictive components for B > 2 T, approximately half that

seen in FeV_2O_4 under similar conditions. This result is in reasonable agreement with strain measurements on MnV_2O_4 by Suzuki et al. [24].

As reported in Ref. [17], with increasing temperature, the anisotropic compression effect and hysteresis decrease, and above 30 K only the isotropic magnetostriction persists up to the transition temperature region near T_C. Above T_C, the isotropic magnetostriction effect also becomes negligible. Over the temperature range of the measurements the dissipative component, due to the highly localized nature of carriers, does not obscure the magnetocapacitive signal.

We end this section by emphasizing some differences with the FeV_2O_4. First, the anisotropic magnetocapacitive signal in MnV_2O_4 at low temperatures corresponds to a contraction of the sample dimensions along the magnetic field direction, and there is a comparably sized, isotropic magnetostrictive effect. Second, if there is a coercive field, it is very small since neither the isotropic nor anisotropic capacitive signals show extrema away from B = 0 (see also Ref. [21]), and no magnetocaloric signature is observed at the lowest temperature of the measurements. We note that unlike the magnetocaloric effect associated with domain reversal described herein, the temperature dependent spin-entropy, also called a magnetocaloric effect or MCE, shows for polycrystalline MnV_2O_4 differences for different magnetic field values[7]. MCE predicts an adiabatic temperature change of about 0.5 K at 20 K for a field change from 0 to 2 T. However, this may not be directly related to the domain behavior we describe. Third, in contrast to FeV_2O_4, the MR inferred from the dissipation signal is positive at low temperatures, changes sign between 20 and 30 K, and becomes negligible above T_C.

C. CoV_2O_4

The vanadium-vanadium distance in CoV_2O_4 is the smallest in the spinels treated in this investigation, and in a separate work we have shown that the addition of very high pressure can stabilize a metallic state[14]. CoV_2O_4 does not have a long range ordered structural transition, and undergoes only a paramagnetic-to-ferrimagnetic transition at 152 K. However, recent work[8] indicates that there are two additional features at 100 K and 59 K, the latter of which may be due to short range orbital order. Due to the high conductivity of the material, our dielectric studies were limited to temperatures below 30 K; conversely, this allowed us to explore the behavior above 15 K using conventional magnetoresistance measurements.

C.1 Dielectric studies.

In Fig. 8a representative magnetic field dependent capacitance data for a CoV_2O_4 single crystal is shown for 4.3 K ($B \perp E$). Due to the high conductivity the magnetic field dependence of the real and imaginary (not shown) dielectric signals follow each other very closely[17]. From the sharp feature (which is opposite for B//E) at low magnetic fields (± 0.2 T), we find that the sample dimensions contract along the direction of the applied field. This is the same sign of anisotropic contraction seen in MnV_2O_4 (and contrary to that observed in FeV_2O_4). This anisotropic magnetostrictive effect is important, since for the case of CoV_2O_4 the cubic phase remains at low temperature. This would imply that in the presence of a cubic structure there can be no pre-existing tetragonal domains that can align with increasing field, thereby changing the crystal dimensions. However anisotropic magnetostrictive effects do arise, and spin and orbital effects must induce some kind of lattice strain, a possibility supported by distinct features seen in the magnetocaloric effect in this same range of field. Since heat is released in domain reversal, the two signatures clearly show that there are multiple domain effects in the material. The most

likely explanation for lattice-related effects may be the presence of short-range orbital order [8] which may occur below 59 K.

Above about 0.2 T, the dielectric signal becomes strongly affected by magnetoconductance effects, and history and time dependent. As shown in Fig. 8b and 8c, we have done magnetic field cycles where we stop the field and observe the relaxation of the dielectric response. The relaxation data are best described by a modified stretched exponential formulation: $C(t) = C_0 + C_1 t^{-\alpha} \exp(-(t)^{\beta}/\tau)$, which combines an empirical power law($t^{-\alpha}$) and a stretched exponential ($\exp(-(t)^{\beta}/\tau)$) decay behavior. Fits of $C(t)$ to the data in Fig. 8c yield the parameters α, β, and τ of order 0.0, 0.9, and 1000 respectively at 4.5 K (i.e. nearly exponential), and 0.2, 0.1, and 2 respectively at 8 K (i.e. power law dominated). These parameters are not strongly field-dependent. Provided a glassy state describes the behavior, we estimate that the corresponding glass transition to be about $T_g \sim 10$ K. In contrast to the other two spinels studied, CoV_2O_4 exhibits a slight frequency dependence of the temperature dependent dielectric response[17] characteristic of electric dipole (Debye) relaxation[25]. Arrhenius analysis indicates a dipole oscillator with a characteristic energy of about 20 meV.

How electric dipole excitations, charge carriers, and the magnetic ground state and lattice interact to produce the unusual behavior of this material at low temperatures is not clear. Huang et al. propose that below 59 K there is a spin-glass state, based on the frequency dependence of the ac susceptibility and the FC and ZFC magnetization[8], due perhaps to short-range orbital order. Our results for both the time and frequency dependent features may be a manifestation of this since we know that the magnetization (and thereby the susceptibility) can couple to the dielectric response.

C.2) Electrical transport studies.

In Fig. 9a, the magnetoresistance (MR = (R(B)–R(0))/R(0)) taken with standard 4-terminal electrical transport methods is shown for I⊥B up to 6 T, and in Fig. 9b the MR vs. temperature at 6 T is summarized. Starting at 15 K, the MR first rises to 20 K, and then drops rapidly with increasing temperature until 50 K, then decreases more slowly, changes sign around 100 K, and finally shows a kink at the magnetic transition T_C. We note that the magnetoconductivity (i.e. negative slope of ε'' vs. B above 0.2 T) seen in dielectric measurements[17] corresponds to the positive magnetoresistance (MR) in Fig. 9 in the 10 to 30 K range. Although in CoV_2O_4 there is only one known magnetic transition, and no known structural transitions, the temperature dependent features in the MR appear to involve both magnetic and structural aspects of the apparently complex low temperature nature of CoV_2O_4 suggested in Ref. [8].

IV. DISCUSSION

IV.1. Magnetostriction

We first compare the magnetostrictive properties of the three spinel compounds investigated at temperatures below their lowest respective magnetic transitions. Our measurements show that along the direction of the magnetic field, only in the case of FeV_2O_4 does the lattice expand, whereas for MnV_2O_4 and CoV_2O_4 the lattices contract. By considering the re-alignment of tetragonal micro-domains in the magnetic hysteresis data, where the c-axis always aligns with the magnetic field, an expansion is expected when c > a, and a compression when c < a; and based on previous experimental and theoretical work, this is indeed the case for FeV_2O_4 and MnV_2O_4 respectively. Katsufuji et al.[9], and later Zhang et al. [5] have considered in detail the interaction of the Fe tetrahedral and V octahedral sites in terms of orbital ordering,

lattice distortions, and magnetic exchange energies (i.e. $J_{A\text{-}B}$) and conclude that the low temperature tetragonal configuration is the result of orbital effects on the A and B sites where both the tetrahedral and octahedral structures undergo cooperative distortions leading to c > a (here c is in the tetragonal structure, and a is in the original cubic frame of reference). A more detailed description of the orbital effects has recently been treated using density functional theory (DFT)[4] where they conclude that there are two possible tetragonal configurations when both the A and B sites have orbital degrees of freedom, as in FeV_2O_4, leading to c > a in the low temperature tetragonal phase. In contrast, where only the B site has orbital ordering, the low temperature tetragonal phase remains as c < a, which is the case for MnV_2O_4, consistent with the present and previous experimental work[21, 22, 24].

Although CoV_2O_4 does not have a low temperature tetragonal phase, at least with long range order, it does exhibit an anisotropic compression at low fields and temperatures, based on the simple interpretation of the capacitive response for B//E and B⊥E. The presence of short-range orbital order as proposed by Huang et al. [8] may explain the relatively weak, but evident presence of anisotropic compression (i.e. a "c < a tendency") for CoV_2O_4, which would be expected with orbital order only on the B site. (See also *IV.4*.)

An additional finding in the case of MnV_2O_4 is the very pronounced *isotropic* compression with magnetic field intensity. For MnV_2O_4, neutron[22] and NMR[21] studies both suggest a staggered arrangement of the V orbitals, with two in-equivalent sites in the pyrochlore sublattice. However, it is not clear at present how this structure alone would lead to the two different types of magnetostrictive signals (anisotropic and isotropic) we find. If the Mn-V coupling is not too large, the Mn site (or more generally the A-site), may play an independent Zeeman-type isotropic magnetostrictive role in parallel with the anisotropic nature of the orbital V-site. (See also *IV.2.)*

Hence similar isotropic magnetostriction may occur in the other two compounds, but must be significantly less than the pronounce effect seen in MnV_2O_4.

IV.2 Coercive field and independent magnetic effects.

Evidence for independent magnetic effects in these materials comes from the appearance of multiple coercive fields at low temperatures. In FeV_2O_4, the larger is $B_c \sim 1$ T, and the smaller is $B_c' \sim 0.01$ T. In CoV_2O_4, subtle changes in C and the magnetocaloric effect occurred at $B_c \sim 0.1$ T and $B_c' \sim 0.03$ T. For MnV_2O_4, there is a saturation field, but no B_c is observed. However, even up to temperatures of order T_s and T_C, very small anomalies in C are evident at very small fields, corresponding to a $B_c' \sim 0.15$ T (not shown, see [17]). The absence of B_c in MnV_2O_4 has been observed in the magnetization data reported by Luo et al. [7], and explained by Baek et al.[21] as a decoupling of the lattice and magnetic domain structure in field. This model may help explain the coexistence of isotropic and anisotropic magnetostrictive effects in MnV_2O_4 since the magnetic structure can always align along the field direction (isotropic), whereas orbital-lattice structure is locked into the lattice (anisotropic).

IV.3 Canted spin structure and FeV_2O_4 in high magnetic fields.

In Fig. 6 we observed a continuous change in the magnetization (via ΔC) in FeV_2O_4 at 1.5 K between 5 and 30 T. In the low field hysteresis cycle below 5 T, the change in ΔC is due mainly to domain orientation effects, and the non-collinear structure[3, 16] of the Fe-V spin structure. However, at higher fields, it may be possible for the canted spin structure to change, and this may be reflected in the behavior of the high field dielectric response in Fig. 6. (The field and energy scale for changes in the ferrimagnetic structure should be correlated with the A-B site interaction $J_{A\text{-}B}$.) This possibility is supported by recent electric polarization studies that show

that FeV_2O_4 exhibits a significant ferroelectric effect below T_{OT} [5]. In Ref. [5] the authors suggest that the non-collinear nature of the spin structure leads to the ferroelectric polarization through a Dzyaloshinskii-Moriya type interaction (i.e. $\mathbf{P}_{ij} = a\boldsymbol{\varepsilon}_{ij} \times (\mathbf{S}_i \times \mathbf{S}_j)$ where S_i and S_j are adjacent V^{3+} spins, $\boldsymbol{\varepsilon}_{ij}$ is the vector between the spins, and $\mathbf{P}_{ij}$ is the polarization[26]. An important feature of the polarization is that it is suppressed with increasing magnetic field, directly affecting the cross product and thereby the polarization. Hence it is possible that at high fields well above the reorientation saturation field of the ferrimagnetic domains, the non-collinear spin structure begins to change, and thereby the magnetodielectric signal also undergoes further changes. Eventually, at high enough magnetic fields, the Fe-V canted spin structure could become ferromagnetically polarized as in $CdCr_2O_4$ and $ZnCr_2O_4$[27]. Similar high magnetic field effects in the magnetocapacitance signal in MnV_2O_4 might also be observable since this spin system is also canted at low temperature.

IV.4 The special case of CoV_2O_4.

CoV_2O_4 may be the least well understood, but most interesting vanadate spinel investigated in the present work. Although no structural transition occurs in CoV_2O_4 at the ferrimagnetic transition $T_C = 152$ K, Huang et al. [8] have discovered in polycrystalline samples two additional distinguishing properties of CoV_2O_4 at 100 K and at $T_1 = 59$ K, both observed as dips in the thermal conductivity. Below 100 K, differences in the FC and ZFC magnetization appear, and near T_1 there is a weakening and broadening of the XRD spectrum, and anomalies appear in the specific heat and magnetization. Below T_1, the susceptibility is frequency dependent, where the peak in the loss tangent goes like $\ln(f) \sim E_a/k_BT$ (the activation energy is $E_a = 60$ meV). The authors discuss the possibility of a spin-glass state (polycrystal) or "orbital-glass" state (single

crystal) below T_1 which may be due to short range orbital order. In our results the following comparisons with the data of Ref. [8] can be made. First, in our magnetoresistance data, we see changes in the slope and/or sign of the MR near 20 K, 50 K, 100 K, and 160 K (Fig. 9), which except for 20 K, roughly correspond to the transitions observed in Ref. [8]. Second, the time-dependent behavior of the magneto-dielectric response that becomes very clear below 10 K is additional evidence for a low temperature glassy state, the dynamic behavior of which is clearly coupled to the magnetic field. Third, the frequency dependence of the resonance in the dielectric response[17], like the ac susceptibility, also follows a $\ln(f) \sim E_a/k_BT$ rule, but here E_a is about 3 times less (20 meV). Although the connection between these two measurements (i.e. χ vs. ε) is tenuous, they may both be coupling via spin-orbital-lattice interactions to short range dynamics below T_1. Hence the frequency dependence of the dielectric response, not seen in the other two compounds, may arise from a process analogous to, but of a different origin than a conventional electronic dipole. As far as we can discern from our measurements, only CoV_2O_4 shows a pronounced example of glassy behavior in the low temperature magneto-dielectric response.

V. SUMMARY AND CONCLUSIONS

Simple dielectric measurements show many of the changes in magnetic and structural order in single crystal vanadate spinels, complementing magnetization, specific heat, XRD, and other methods. This simplicity facilitates measurements at both very low temperatures and high magnetic fields, and hence magnetic and structural information is accessible under these extreme conditions. Where the electrical conductivity at low temperatures is too low for conventional electrical transport measurements in the semiconducting spinel compounds, the dissipative dielectric signal further yields information on the magnetoconductivity which is complementary to conventional magnetoresistance measurements only possible at higher temperatures. The main

findings of the present work, based on these dielectric studies are: (*i*) In single crystals at low temperatures, the magnetocapacitance is highly representative of the behavior of the magnetic hysteresis obtained by magnetization methods, including the remnant and coercive field signatures, and through magneto-caloric signatures that appear due to temperature transients, details associated with magnetic domain changes. These signatures were particularly evident in the cases FeV_2O_4 and CoV_2O_4. In the former case, the signatures are consistent with magnetization where it is possible that the V and Fe orbital-lattice effects have different coercive fields, but in the latter case the appearance of any domain-like behavior related to the lattice is anomalous since the tendency for a structural transition is highly suppressed. (*ii*) Above the saturation fields of the hysteresis cycles, the magnetocapacitance FeV_2O_4 exhibits a further, monotonic change which was studied up to 33 T at 1.5 K(Fig. 6). We speculate that this may be related to an alteration of the non-collinear spin structure with increasing magnetic field, but further work will be necessary to confirm this. (*iii*) By performing measurements vs. magnetic field direction, it is possible to separate the isotropic and anisotropic magnetostrictive effects, which were most dramatic in the case of MnV_2O_4. This is important to our understanding of the spin and orbital behavior (and their interactions) due to the Zeeman (isotropic) and orbital (anisotropic) nature of the magnetic structure in these materials. (*iv*) A time dependent magnetocapacitive signal was observed in CoV_2O_4 that exhibited a temperature dependent stretched-exponential behavior, which vanished above 10 K. We describe this as a glass-like behavior since at present it is unclear how spin and/or orbital effects may be acting, and due to the proximity of CoV_2O_4 to the itinerant electron threshold, the electrical conductivity may also play a role in the behavior. (*v*) Where overlapping comparisons could be made, the MR studied by conventional electrical transport and the inverse of the magnetoconductance from dielectric

measurements were consistent in describing the sign of the MR in different magnetic phases. Hence although these materials are semiconductors, MR can play a major role in future studies since it brings new information about the spin structure (i.e. order and disorder) and highly correlated electronic transport mechanisms (e.g. magnetic polarons [28]).

We conclude by noting that the behavior of the vanadate spinels are highly dependent on the A-site atom, where the various mechanisms including itinerant charge, A-B site coupling, and orbital and spin degrees of freedom contribute to differing degrees in their physical properties. The present work shows that there is still a lot to do to sort out the relative roles of these mechanisms, that low temperatures and high magnetic fields give an advantage to revealing important effects, and that dielectric studies can play an important part in this effort.

ACKNOWLEDGMENTS

We would like to thank A. Kiswandhi for valuable discussions. Work supported in part by NSF-DMR-1005293. A portion of this work was performed at the National High Magnetic Field Laboratory, which is supported by NSF Cooperative Agreement No. DMR-0654118, by the State of Florida and by the DOE.

REFERENCES

[1] A. P. Ramirez, in Handbook of Magnetic Materials, K. H. J. Buschow ed., Elsevier, Amsterdam **13,** 423 (2001).

[2] S.-H. Lee, H. Takagi, D. Louca, M. Matsuda, S. Ji, H. Ueda, Y. Ueda, T. Katsufuji, J.-H. Chung, S. Park, S.-W. Cheong, and C. Broholm, J. Phys. Soc. Japan **79,** 011004 (2010).

[3] G. J. MacDougall, V. O. Garlea, A. A. Aczel, H. D. Zhou, and S. E. Nagler, Phys. Rev. B **86,** 060414 (2012).

[4] S. Sarkar and T. Saha-Dasgupta, Phys. Rev. B **84,** 235112 (2011).

[5] Q. Zhang, K. Singh, F. Guillou, C. Simon, Y. Breard, V. Caignaert, and V. Hardy, Phys. Rev. B **85,** 054405 (2012).

[6] K. Myung-Whun, S. Y. Jang, T. Katsufuji, and A. V. Boris, Phys. Rev. B **85,** 224423 (2012).

[7] X. Luo, Y. P. Sun, L. Hu, and B. S. Wan, J. Phys.: Condens. Matter **21,** 436010 (2009).

[8] Y. Huang, Z. Yang, and Y. Zhang, J. Phys.: Condens. Matter **24,** 056003 (2012).

[9] T. Katsufuji, T. Suzuki, H. Takei, M. Shingu, K. Kato, K. Osaka, M. Takata, H. Sagayama, and T.-h. Arima, J. Phys. Soc. Japan Lett. **77,** 053708 (2008).

[10] Z. Zhang, D. Louca, A. Visinoiu, S. H. Lee, J. D. Thompson, T. Proffen, A. Llobet, Y. Qiu, S. Park, and Y. Ueda, Phys. Rev. B **74,** 014108 (2006).

[11] S. Blanco-Canosa, F. Rivadulla, V. Pardo, D. Baldomir, J. S. Zhou, M. Garcia-Hernandez, M. A. Lopez-Quintela, J. Rivas, and J. B. Goodenough, Phys. Rev.Lett. **99,** 187201 (2007).

[12] A. Kiswandhi, J. S. Brooks, J. Lu, J. Whalen, T. Siegrist, and H. D. Zhou, Phys. Rev. B **84,** 205138 (2011).

[13] S. Sarkar, T. Maitra, R. Valenti, and T. Saha-Dasgupta, Phys. Rev. Lett. **102,** 216405 (2009).

[14] A. Kismarahardja, J. S. Brooks, A. Kiswandhi, K. Matsubayashi, R. Yamanaka, Y. Uwatoko, J. Whalen, T. Siegrist, and H. D. Zhou, Phys. Rev. Lett. **106,** 056602 (2011).

[15] A. V. Andrianov and O. A. Savel'eva, Phys. Rev. B **78,** 064421 (2008).

[16] J. S. Kang, J. Hwang, D. H. Kim, E. Lee, W. C. Kim, C. S. Kim, S. Kwon, S. Lee, J. Y. Kim, T. Ueno, M. Sawada, B. Kim, B. H. Kim, and B. I. Min, Phys. Rev. B **85,** 165136 (2012).

[17] A.Kismarahardja, **http://etd.lib.fsu.edu/theses/available/etd-11042010-162636/** Ph.D.Thesis, Florida State University (2010).

[18] S. Nishihara, W. Doi, H. Ishibashi, Y. Hosokoshi, X.-M. Ren, and S. Mori, J. Appl. Phys. **107,** 09A504 (2010).

[19] H. Takei, T. Suzuki, and T. Katsufuji, Appl. Phys. Lett. **91,** 072506 (2007).

[20] H. D. Zhou, J. Lu, and C. R. Wiebe, Phys. Rev. B **76,** 174403 (2007).

[21] S. H. Baek, N. J. Curro, K. Y. Choi, A. P. Reyes, P. L. Kuhns, H. D. Zhou, and C. R. Wiebe, Phys. Rev. B **80,** 140406 (2009).

[22] V. O. Garlea, R. Jin, D. Mandrus, B. Roessli, Q. Huang, M. Miller, A. J. Schultz, and S. E. Nagler, Phys.Rev. Lett. **100,** 066404 (2008).

[23] K. Adachi, T. Suzuki, K. Kato, K. Osaka, M. Takata, and T. Katsufuji, Phys. Rev. Lett. **95,** 197202 (2005).

[24] T. Suzuki, M. Katsumura, K. Taniguchi, T. Arima, and T. Katsufuji, Phys. Rev. Lett. **98,** 127203 (2007).

[25] J. S. Brooks, R. Vasic, A. Kismarahardja, E. Steven, T. Tokumoto, P. Schlottmann, and S. Kelly, Phys. Rev. B **78,** 045205 (2008).
[26] H. Katsura, N. Nagaosa, and A. V. Balatsky, Phys.l Rev. Lett. **95,** (2005).
[27] E. Kojima, H. Ueda, Y. Ueda, A. Miyata, S. Miyabe, and S. Takeyama, Journal of Physics: Conference Series **145,** 012023 (2009).
[28] N. F. Mott and E. A. Davis, *Electronic Processes in Non-Crystalline Materials* (Oxford University Press, London, 1979).

FIGURE CAPTIONS

Figure 1. (Color online) Spinel structure of AB_2O_4. (a) Cubic cell (a ~ 8.5 Å) showing tetrahedral (A) and octahedral (B) ion sites. (Apical oxygen's not shown.) (b) Underlying pyrochlore structure of the B ion sites. (a) Ferrimagnetic transition temperature (T_C) vs. inverse V-V distance $1/R_{V\text{-}V}$ and activation energy E_a derived from temperature dependent resistance above T_C.

Figure 2. (Color online) General features of single crystal samples of AV_2O_4 (A = Mn, Fe, and Co). (a) Temperature dependent resistivity. CoV_2O_4 is nearest to the itinerant electron regime, and this allows a clear signature of T_C to be easily seen in the (smaller) resistivity measurement. (b,c) Temperature dependence of the capacitive ε' (b) and dissipative ε''(c) signals for FeV_2O_4. The positions of the structural transitions derived from x-ray diffraction measurements [9] are shown for reference.

Figure 3. (Color online) Magnetic field dependent capacitance signal of FeV_2O_4 for B⊥E (a) and B//E (b) at 4.2 K. The sharp rises in ΔC near 1 T are due to the magnetocaloric effect and corresponding temperature rise (i.e. dC/dT >0) when the magnetization changes sign at the larger coercive field B_c. Inset of (a): low-field coercive feature B_c' in capacitance signal. (c) Magnetization and converted magnetocapacitance signal for FeV_2O_4 based on the $C \sim M^2$ relation proposed in Ref. [19]. Arrows refer to the direction of hysteresis. B_c is the larger coercive field and B_c' refers to a small coercive feature seen near zero field in the magnetization. Schematics: The two different orientations of the electric and magnetic fields used in the dielectric measurements of the single crystal spinels. The $\mathbf{a_1}$, $\mathbf{a_2}$ and $\mathbf{a_3}$ are the principal axes of

the cubic structure. The small strain from the rotating sample holder used to fix the sample position is always in the direction of the electric field.

Figure 4. (Color online) Magnetodielectric response of FeV_2O_4 for B⊥E for increasing temperature between 4.2 K and T_{LT} transition. (a, b) Percent change in C and D respectively. (c) Magnetocapacitive hysteresis loops derived from $C_{reactive} \sim M^2$ with the dissipative background D removed. The hysteresis loop directions are counterclockwise in all cases.

Figure 5. (Color online) Coercive field B_c in the dielectric response of FeV_2O_4. (a) Magnetocaloric effect (arrows) in ε' for domain switching at different temperatures. (b) Coercive field B_c from magnetocaloric effect in (a), magnetocapacitive signal in Fig. 4c, and magnetization[17]. B_c vanishes at 70 K, near T_{LT}.

Figure 6. (Color Online) Magnetocapacitive signal at fields well above the coercive and saturation fields at 1.5 K (similar to Fig. 3a, but at fields above 5 T). Inset: speculation about how the non-collinear spin configuration[69] may evolve in the high field limit. (After Refs. [36, 37]).

Figure 7. (Color online) Magnetodielectric response ε' and ε" of MnV_2O_4 at 4.3 K for B//E and B⊥E. (a) Original capacitace data for B//E and B⊥E in terms of the change in ε'. (b) Anisotropic capacitance signal extracted from (a). This signal is positive for B//E and negative for B⊥E. (c) Isotropic capacitance signal. This signal is always positive for both B//E and B⊥E. The smaller double peak structure seen for B⊥E in (a) is due to the <u>difference</u> of the isotropic and anisotropic hysteresis signals, whereas the larger single dip structure for B//E in (a) is due to their <u>addition</u>.

Figure 8. (Color online) (a) Magnetocapacitive response of CoV_2O_4 for B⊥E at 4.3 K. Starting at zero field, C decreases with field for B⊥E (down arrow) and ε' increases with field for E//B (not shown), indicating that in the low field range the sample dimensions decrease along the field direction. At higher fields, the capacitance signal is strongly coupled to the magnetoconductance (D)[17]. (b) Comparison of continuous field sweep (dashed line) and stepwise field sweep (solid line) of the capacitance at 4.5 K. Hold times for the stepwise data were of order 4000 seconds. (c) Time dependence of the capacitance change at 1 T for different temperatures.

Figure 9. (Color online) (a,b) Magnetoresistance (MR) of CoV_2O_4 for i⊥B. (c) Temperature dependence of the MR of CoV_2O_4 at 6 T. Although there is no long range order structural transition at 59 K[8], the slope of temperature dependence of the MR seems to change significantly near this temperature. The magnetic transition at T_C is seen as a minimum in the MR data.

FIGURES

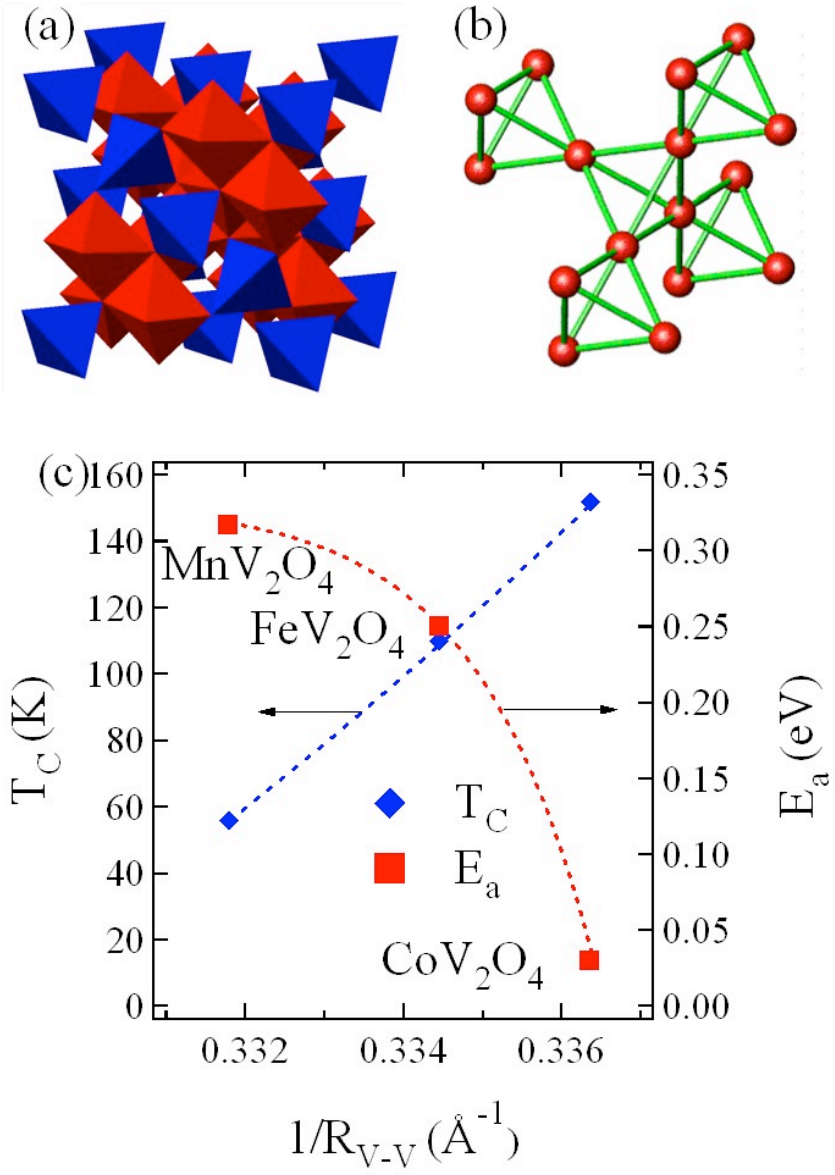

Figure 1 (a,b,c). Kismarahardja et al.

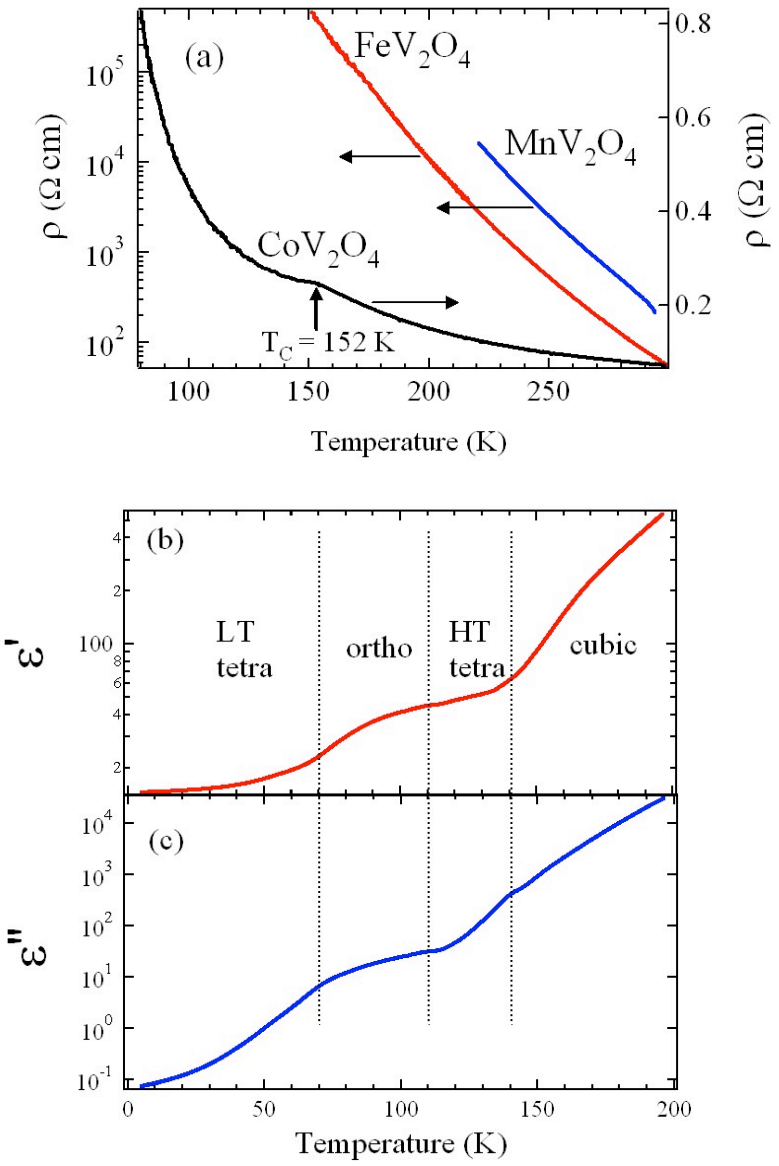

Figure 2 (a,b,c). Kismarahardja et al.

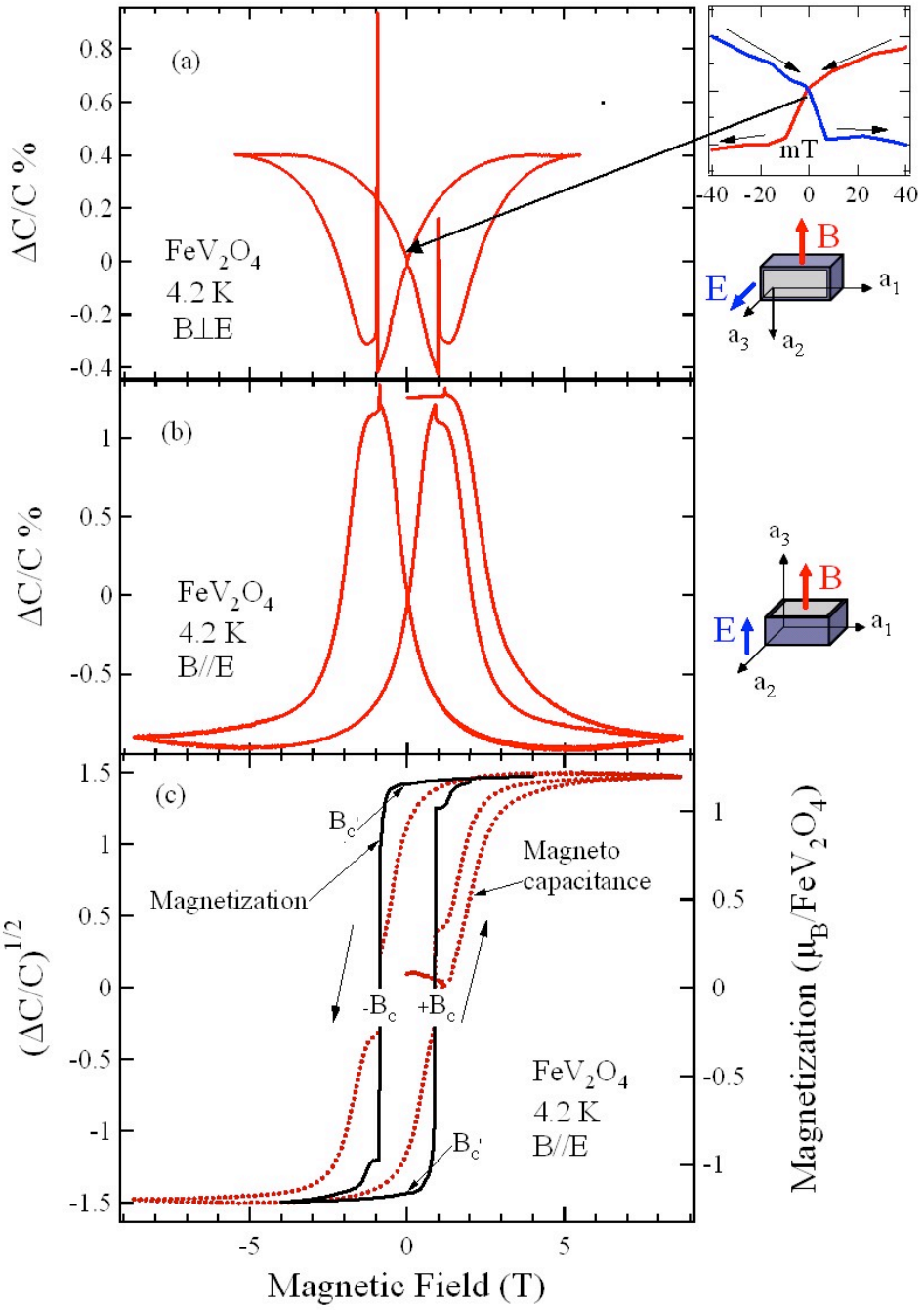

Figure 3 (a,b,c). Kismarahardja et al.

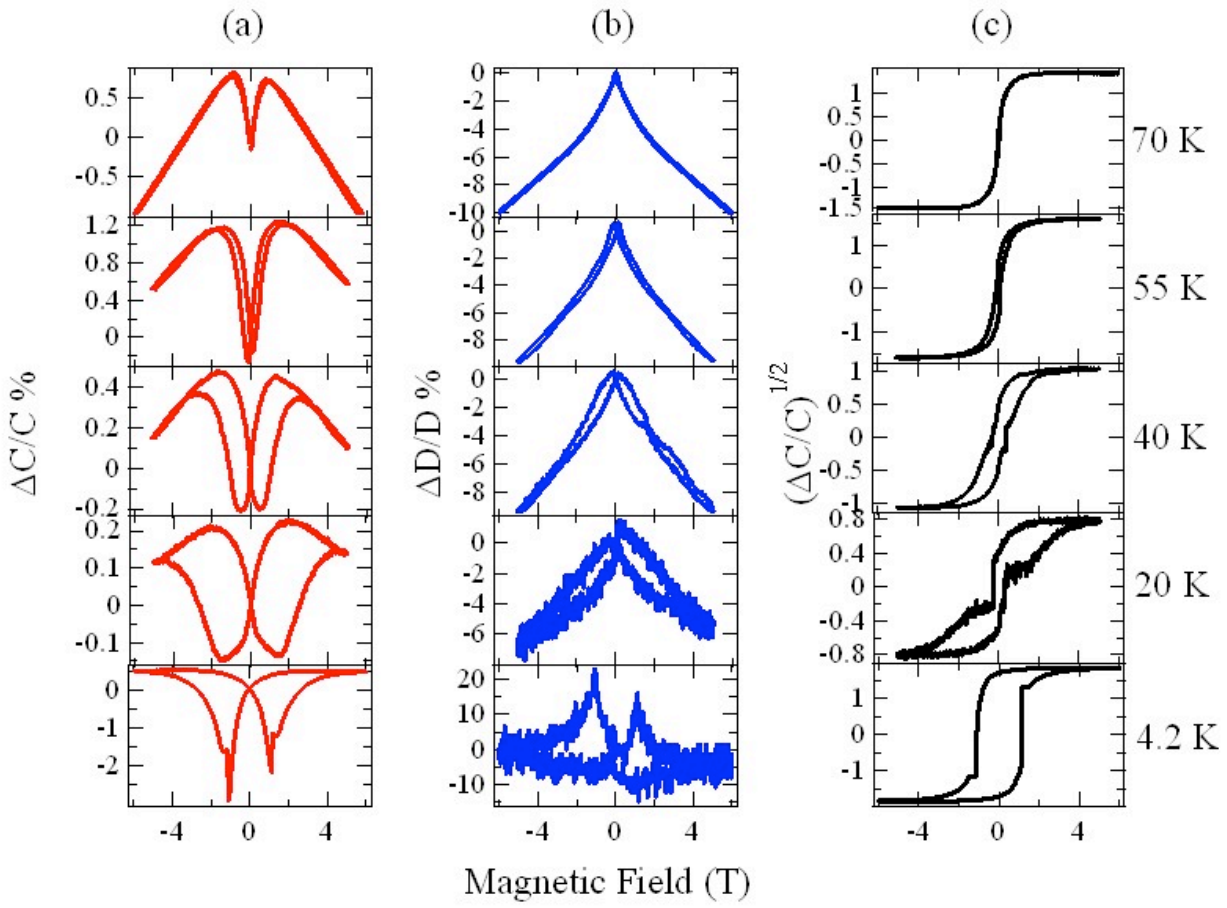

Figure 4 (a,b,c). Kismarahardja et al.

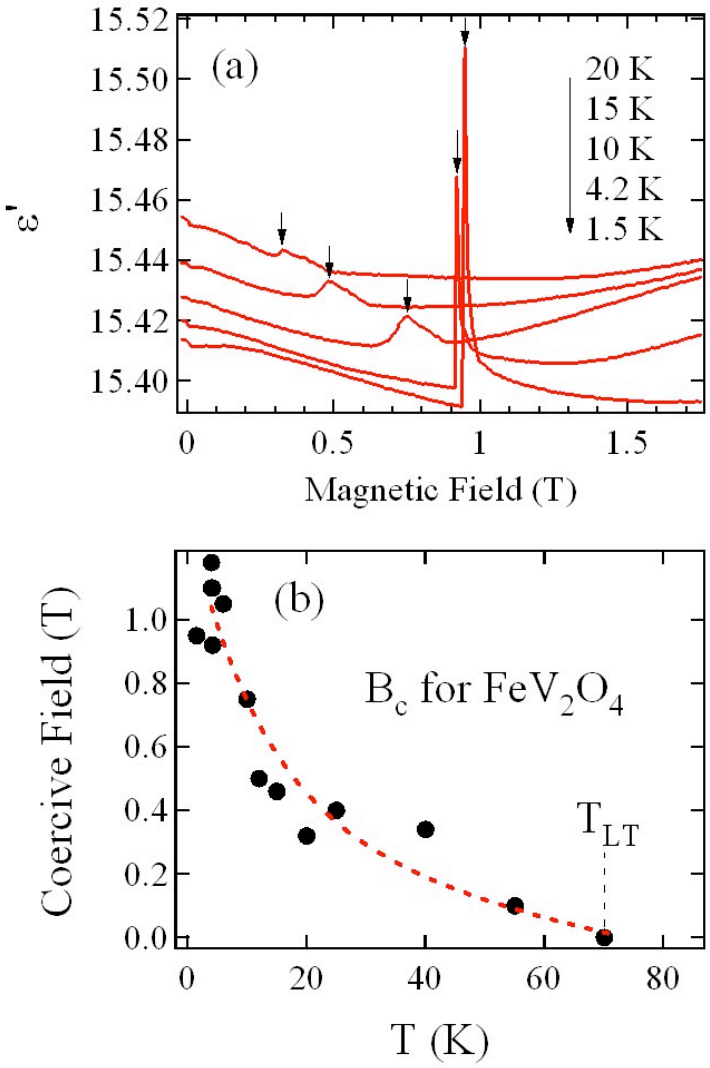

Figure 5 (a,b). Kismarahardja et al.

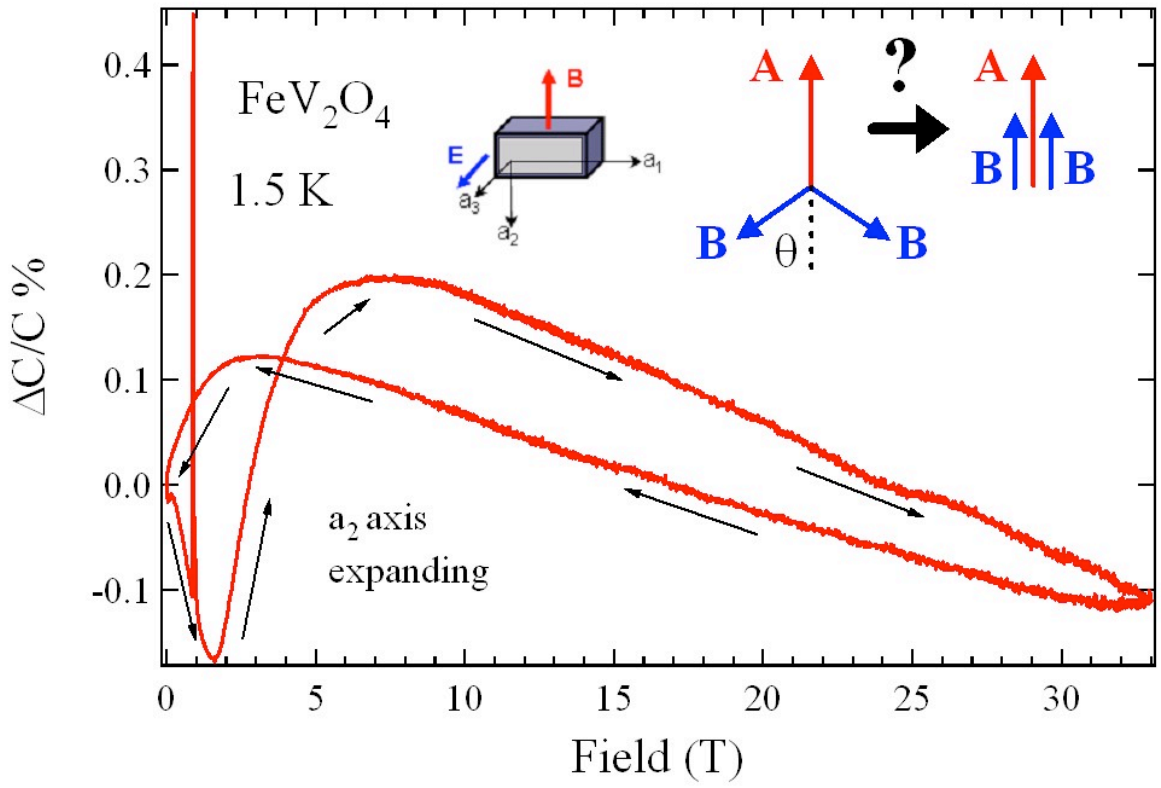

Figure 6. Kismarahardja et al.

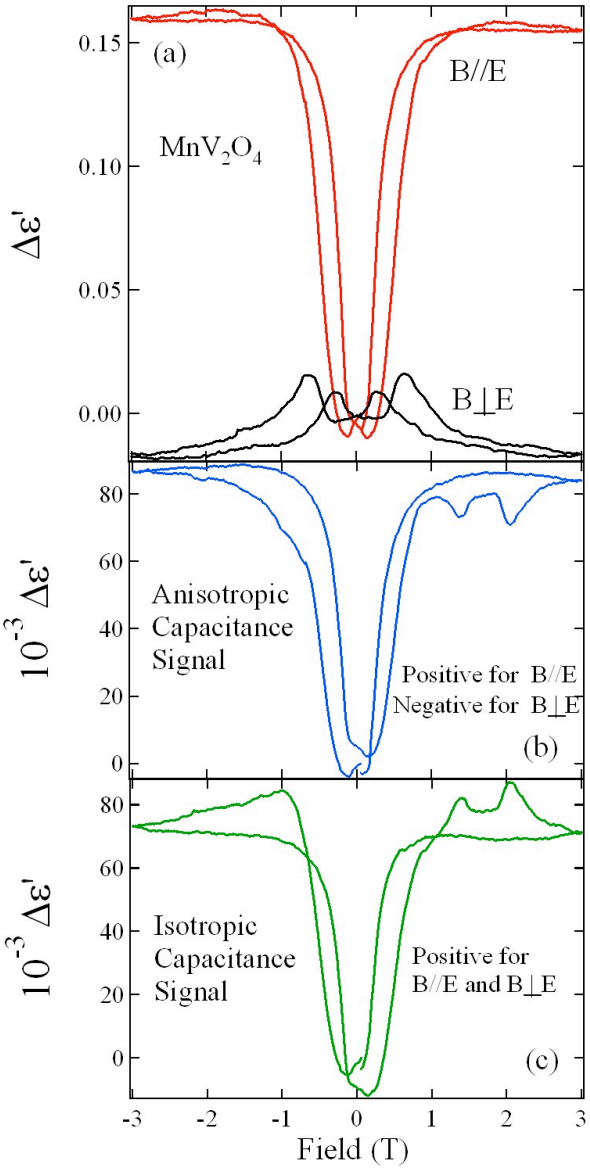

Figure 7 (a,b,c). Kismarahardja et al.

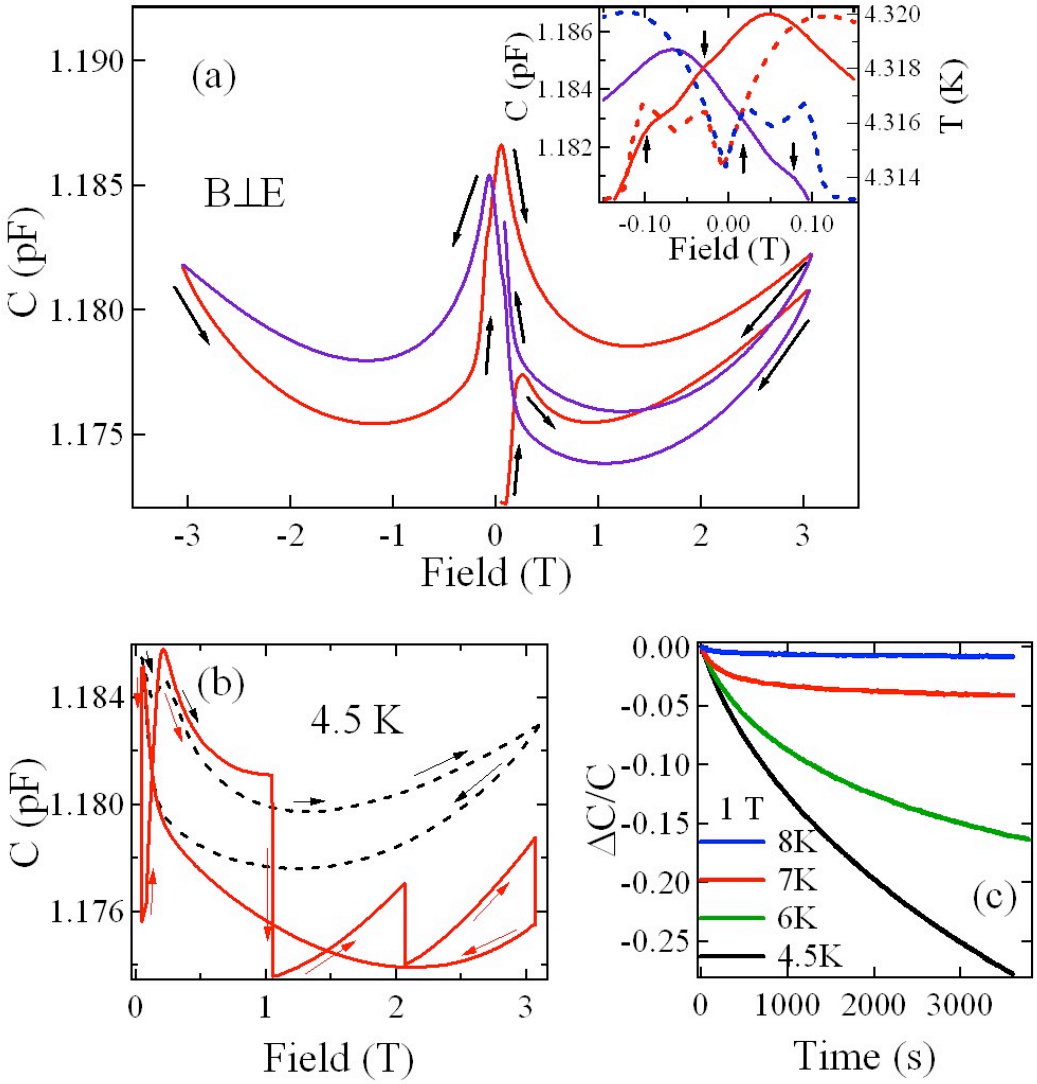

Figure 8 (a,b,c). Kismarahardja et al.

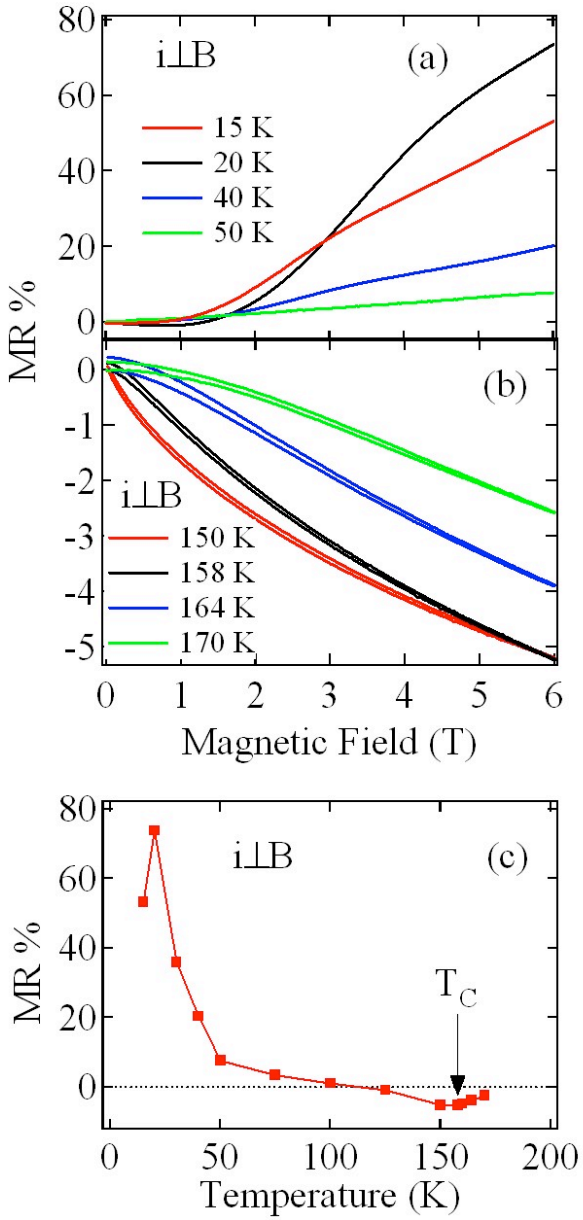

Figure 9 (a,b,c). Kismarahardja et al.